Tenma: Robust Cross-Embodiment Robot Manipulation with Diffusion Transformer

Travis Davies[1], Yiqi Huang[1], Yunxin Liu[2], Xiang Chen[3], Huxian Liu[1], Luhui Hu[1]
[1]ZhiCheng AI, [2]Tsinghua University, [3]Peking University

***Abstract*— Scaling Transformer policies and diffusion models has advanced robotic manipulation, yet combining these techniques in *lightweight*, cross-embodiment *learning* settings remains challenging. We study design choices that most affect stability and performance for diffusion–transformer policies trained on heterogeneous, multimodal robot data, and introduce Tenma, a lightweight diffusion–transformer for bi-manual arm control. Tenma integrates multiview RGB, proprioception, and language via a cross-embodiment normalizer that maps disparate state/action spaces into a shared latent space; a *Joint State–Time* encoder for temporally aligned observation learning with inference speed boosts; and a diffusion action decoder optimized training stability and learning capacity. Across benchmarks and under matched compute, Tenma achieves an average success rate of 88.95% in-distribution and maintains strong performance under object and scene shifts, substantially exceeding baseline policies whose best in-distribution average is 18.12%. Despite using moderate data scale, Tenma delivers robust manipulation and generalization, indicating the great potential for multimodal and cross-embodiment learning strategies for further augmenting the capacity of transformer-based imitation learning policies.**

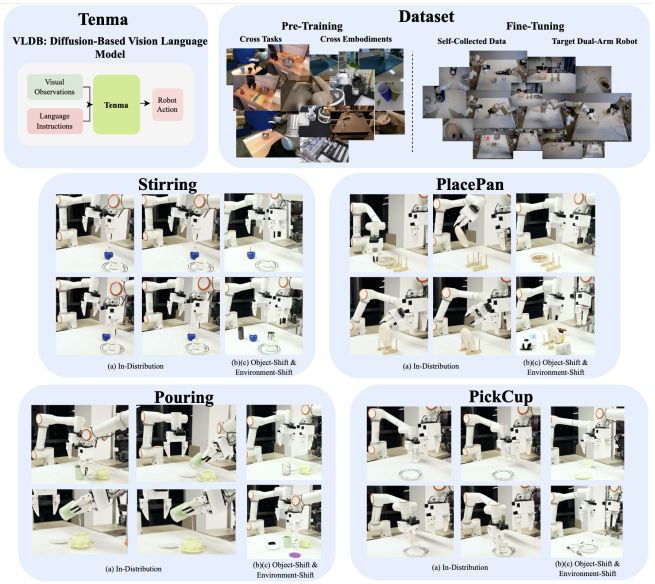

Fig. 1: Overview. Tenma is a diffusion–transformer that learns cross-embodiment representations for robot action generation. The model is pretrained on a curated subset of Open X-Embodiment, spanning diverse robots and tasks, and fine-tuned on four dual-arm tabletop tasks: *Stirring*, *Pouring*, *PlacePan*, and *PickCup*. Evaluation considers three axes of generalization: (a) in-distribution, (b) object-shift, and (c) scene-shift. For each task, the left panels illustrate in-distribution executions, while the top-right and bottom-right panels show performance under object-shift and scene-shift conditions, respectively.

I. Introduction

Transformer-based, imitation learning policies have recently made impressive strides in fine-grained robotic arm manipulation, with scaling behavior akin to that of large language models-where performance improves considerably with more data and model capacity [1], [2], [3], [4], [5], [6], [7], [8]. With millions of robot expert demonstration trajectories now openly available, there is unprecedented potential to develop generalist policies that unify perception, language understanding, and action synthesis across diverse tasks and embodiments [9], [10], [11].

Robotic data introduces two layers of complexity absent in language-only corpora. **First, multimodal learning**: each training sample combines five distinct modalities with mismatched structures. These include spatio-temporal multiview RGB video, temporal robot proprioception and control signals (i.e. robot actions), and static language prompts alongside diffusion timesteps. Building high-capacity, high-throughput models that can *stably* capture fine-grained features from this heterogeneous data remains a major challenge in robot learning. Current approaches tackle this in different ways: some collapse the rich, high-dimensional inputs into a single token or a token-per-timestep representation, sacrificing crucial details [5], [12], [13]. Others apply full self-attention across all modalities, which is computationally expensive and risks stronger signals drowning out weaker ones [3], [14]. In general, lightweight models tend to under-utilize pretrained ViT-based encoders, limiting their potential for rich visual representation learning, while over-relying on simple attention mechanisms for extracting observation features and using vanilla cross-attention to condition actions on these features.

Second, cross-embodiment heterogeneity: Robotic platforms differ widely in their control representations, from joint angles and quaternions to end-effector poses, and span both uni-manual and bi-manual configurations. A truly generalist policy must therefore map these highly heterogeneous embodiment-specific signals into a unified latent representation and structure, enabling knowledge transfer across platforms rather than interference. Despite recent progress, this remains an unsolved challenge. Many existing models are pretrained or can only be trained on a single embodiment, such as a uni-manual arm [12], [13], [14], [15]. Others disregard critical details such as the ordering and

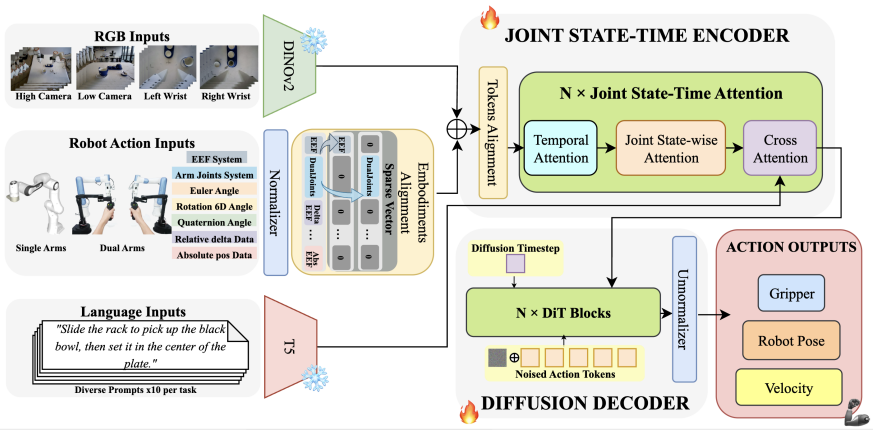

Fig. 2: Overview of the Tenma architecture. The left panel depicts **cross-embodiment normalizer** and frozen multimodal **tokenizers** for vision, language, and proprioception. The top-right module represents the **Joint State–Time Encoder**, which integrates temporally aligned observation tokens with language conditioning. The bottom-right module shows the **DiT-based decoder**, which iteratively denoises action tokens, while the final block illustrates the predicted action sequence structure.

dimensionality of RGB, proprioceptive, and action vectors [3], [6]. An alternative is to assign each embodiment its own token projector to embed data into a shared latent space, but this design scales linearly in spatial complexity with the number of supported embodiments, creating significant overhead [1], [16].

We present **Tenma**, a lightweight diffusion-transformer architecture that learns robust features from cross-embodiment platforms to generate actions in diverse environments. Our work demonstrates that our model can complete tasks in complex settings on a given bi-manual robot arm. Our contributions are as follows:

- A new lightweight transformer model which outperforms previous state-of-the art models across complex bi-manual robot arm tasks.
- New robot learning techniques for robust features from highly multimodal, cross-embodiment data while maintaining high inference frequency and stability. These include our Joint State-Time Attention for flexible and low-latency observation learning across embodiments, our data standardization techniques for embodiment unification, and our hybrid-conditioning diffusion decoder architecture for stable action sampling.
- A detailed evaluation of state-of-the-art models across a set of diverse challenges, with metrics that test abilities beyond simply success rate.

II. Related Work

Scaling robot demonstration data. Inspired by the scaling trends in natural language processing, robotics has similarly pursued large-scale demonstration learning. However, real-world robot data collection remains expensive and logistically difficult [17]. Two primary strategies have emerged: (i) open-source, real-world datasets such as DROID [11], Open X-Embodiment [9], and AgiBot-World [10], which fuel generalist policies like Pi0 [1] and LBM [5]; and (ii) simulation-based pipelines leveraging environments like MuJoCo [18], Isaac Gym [19], and Isaac Sim [20], as adopted by models like Gr00t-N1 [16]. Despite these efforts, learning from diverse datasets remains challenging due to heterogeneity in robot embodiments, sensor modalities, and camera configurations [9]. These inconsistencies hinder the ability of models to learn a unified representation across tasks and platforms. Furthermore, established lightweight policies often lack systematic strategies for handling embodiment diversity at the data level [3], [12], [13], [21]. In this work, we leverage a diverse set of Open X-Embodiment robot demonstrations to learn cross-embodiment features, as well as introduce a data standardization strategies that facilitate consistent learning across heterogeneous platforms for a lightweight robot transformer.

Transformer-based robot policies. Transformer architectures are now central to imitation learning policies, with models such as ACT [21], RT-1 [22], RT-2 [4], and OpenVLA [6] demonstrating the potential of sequence modeling for action generation. More recently, diffusion- and flow-based models [1], [2], [3], [12], [13], [23], [24], [25] have improved policy robustness by enabling diverse action sampling over complex observation spaces. However, these architectures often rely on either collapsing multi-modal features into a single token or applying full-sequence self-attention that can induce information bottlenecks and poor cross-modal integration. Moreover, most lightweight transformer policies continue to rely on ResNet backbones [26] that lack the spatial capacity of modern vision transformers [3], [12], [13], [21]. While pretrained ViTs such as DINO [27] and CLIP [28] have shown strong generalization in other domains, their use in lightweight robotics models remains limited. In this work, we propose new observation feature extraction techniques that exploit the DINOv2 [29] vision and T5 [30] language features for richer feature extraction. What's more, we provide new observation learning and action diffusion

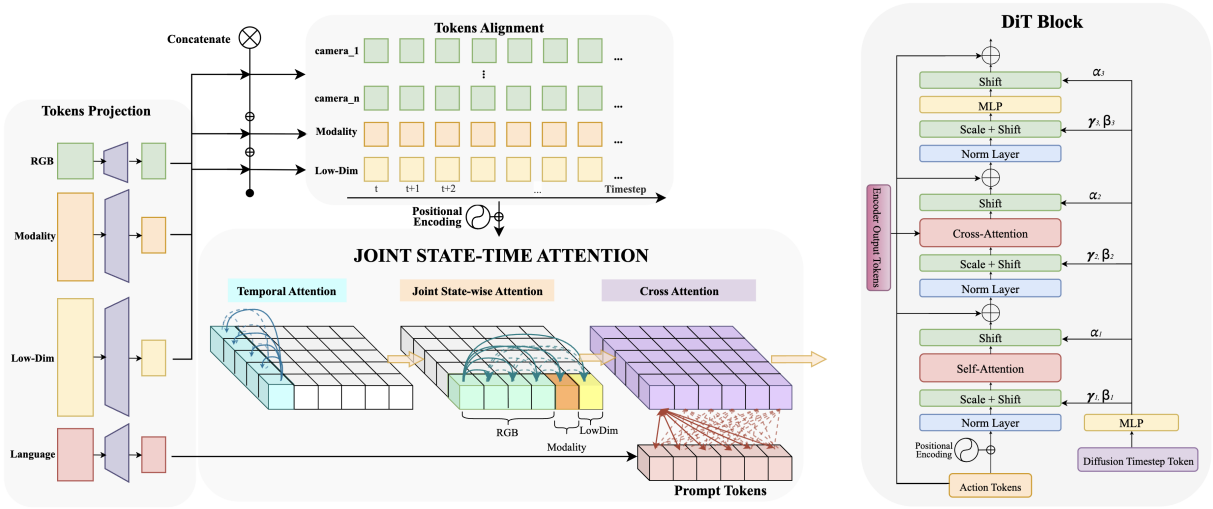

(a) (b)

Fig. 3: Overview of the Tenma encoder–decoder architecture. (a) illustrates the encoding pipeline, where cross-embodiment observations are projected into tokens, temporally aligned, and separated with a **modality token** to encode structural cues and handle variable token lengths across embodiments. These tokens are processed by **Joint State–Time Attention** for multimodal, temporal feature extraction and conditioned with language tokens. (b) depicts the **DiT block**, where noised action tokens are adaptively normalized via **AdaLN** using the diffusion timestep token and refined through **cross-attention** with encoded observation features.

conditioning techniques that outperform previous works by learning more robust, expressive features while maintaining high inference speeds.

III. Problem Formulation

The goal of our diffusion-based policy is to generate a sequence of goal-directed robot joint/Cartesian state actions conditioned on both natural language instructions and recent multimodal sensor observations. This formulation supports generalization across diverse robot embodiments and tasks by unifying perception, language understanding, and action synthesis within a single generative framework.

Specifically, let $\mathcal{L}$ denote the space of language commands, $\mathcal{X}$ the space of RGB video observations, and $\mathcal{Z}$ the space of proprioceptive states. At each time step $t \in \mathbb{N}^+$, the input to the policy is defined as:

$$(\ell, o_t) \in \mathcal{L} \times \left(\mathcal{X}^h \times \mathcal{Z}^h\right),$$

where ℓ is a natural language instruction, and $o_t = (X_{t-h+1:t},\ z_{t-h+1:t})$ represents an h-step observation window with $X_{t-h+1:t} \in \mathcal{X}^h$ denoting RGB frames and $z_{t-h+1:t} \in \mathcal{Z}^h$ denoting proprioceptive states.

The policy π is defined as a function:

$$\pi : \mathcal{L} \times \mathcal{X}^h \times \mathcal{Z}^h \to \mathcal{A}^n,$$

where $\mathcal{A}$ is the action space and n is the prediction horizon. The output sequence $a_{t:t+n-1} = (a_t, a_{t+1}, \ldots, a_{t+n-1})$ consists of future actions aimed at fulfilling the task encoded by ℓ.

A. Training Objective

We instantiate π as a conditional Denoising Diffusion Probabilistic Model (DDPM) [31], a class of generative models that synthesize outputs by reversing a gradual noising process. At each denoising step k, a noisy action trajectory a_k is updated via:

$$a_{k-1} = \alpha\left(a_k - \gamma\,\epsilon_\theta(a_k, k, o_t, \ell)\right) + \mathcal{N}(0, \sigma^2 I),$$

where ϵ_θ is the noise prediction network, and α, γ, and σ are parameters from a predefined diffusion schedule. The model is trained to minimize the discrepancy between the true noise ϵ_k and the predicted noise:

$$\mathcal{L}_{\text{diffusion}} = \|\epsilon_k - \epsilon_\theta(a_t + \epsilon_k,\ k,\ o_t,\ \ell)\|_2^2,$$

with $\epsilon_k \sim \mathcal{N}(0, I)$. Training is performed with $k = 1000$ diffusion steps using a cosine noise schedule [32], while inference is accelerated using deterministic sampling [33] with $k = 7$ steps.

IV. Tenma Model

Tenma is a ViT-based [34] diffusion model designed for cross-embodiment robotic arm control. The architecture adopts an encoder–decoder structure: a Joint State–Time Encoder fuses multimodal observations with language prompts, while a diffusion decoder iteratively denoises future action sequences. To enable multitask learning across diverse embodiments, Tenma employs embodiment-normalization strategies that map heterogeneous joint configurations, camera viewpoints, and sensor layouts into a unified representation. The model is parameter-efficient, pairing a T5-small language encoder with ViT-S-sized transformer blocks for both encoder and decoder. For stability, we employ RMSNorm [35] and QKNorm [36] throughout all non-frozen modules of the network.

A. Proprioceptive & Action Data Standardization

We use a single **cross-embodiment standardizer**: map each robot state into a fixed-length table of canonical slots (e.g., joint angles/velocities, gripper, end-effector pose) with a binary mask for active entries, then apply per-embodiment min–max scaling to $[-1, 1]$, with statistics kept in a dynamic, hashable store and inverted at deployment. This yields a constant-size, embodiment-agnostic token that stabilizes training across robots while avoiding the linear memory growth of per-embodiment projectors [1], [16].

B. Input Tokenization, Encoding & Alignment

Tenma converts each input stream into a sequence of tokens using modality-specific tokenizers (Table I). Each tokenizer maps inputs to a token sequence of shared latent space using modality-specific, two-layer MLPs with RMSNorm [35] and GELU [37]. All tokens are projected to a fixed embedding dimension of 384, ensuring compatibility for transformer-based processing in subsequent modules.

TABLE I: Modality-specific tokenization methods in Tenma.

Modality	Method	Details
RGB (multiview)	DINOv2-S [29]	Retains full patch sequence (no pooling) for robust, object-centric cues [38].
Language	T5-S [30]	Produces contextualized prompt tokens for conditioning.
Proprioception	Standardization	Aligns joint angles, velocities, and gripper states into a unified token with set positions, with a positional mask indicating which features are active at each timestep.

Temporal and spatial positions are encoded using sinusoidal embeddings [39]. Observation data (RGB and proprioceptive sensor data) is temporally aligned to form a unified sequence for transformer processing (Figure 3). To handle variable camera counts across embodiments, a learnable modality token is inserted after each RGB block per timestep, marking modality boundaries for length-invariant fusion without padding. The resulting token sequence serves as the conditioning input for the diffusion process, guiding the denoising of action tokens.

C. Observation Understanding

Observation understanding occurs by performing self-attention and language conditioning on the tokenized observation data. This is performed in the Joint State-Time-Encoder (Figure 2). This module utilizes our Joint State-Time Attention mechanism to factorize attention across time, state, and language to improve efficiency and stability when processing multimodal, cross-embodiment inputs. Each block applies: (1) **Temporal attention** along the time axis with a causal mask to preserve temporal ordering, enabling motion modeling without the quadratic cost of full attention. (2) **Joint state attention** within each timestep, where observation tokens perform joint self-attention. To support *flexible cross-embodiment fusion* with variable RGB token sequence lengths, the *modality token* signals the joint position between the two modalities. This attention is bidirectional, as no temporal constraints exist within a state. (3) **Cross-attention with language tokens**, applied bidirectionally to condition observation features on task prompts, guiding the attention to extract task-oriented features in the observation data.

Full attention scales quadratically with sequence length:

$$\text{Full Attention: } O\big((TS + L)^2\big),$$

where T, S, and L denote timesteps, tokens per state, and language tokens, respectively. Our factorized design reduces this to:

$$\text{Ours: } O(T^2S + S^2T + TSL),$$

eliminating the $O(T^2S^2)$ term and retaining efficient conditioning since $L \ll TS$. This factorization substantially improves inference efficiency while preserving performance comparable to full attention. Inference speed comparisons are shown in Table IV.

D. Action Sampling with Diffusion

Tenma adopts a DiT-style transformer [40] adapted for robotic action denoising (Figure 3). Each block conditions on (i) the encoded observation sequence via **cross-attention** and (ii) a diffusion-timestep embedding through **AdaLN-zero**-based shift-and-scale modulation. This design enables *stable*, *structure-preserving* fusion of multimodal information; allowing each modality to contribute proportionally during the denoising process.

Self-attention among action tokens is bidirectional, while cross-attention to observation tokens is applied within corresponding timesteps to maintain temporal consistency. The decoder terminates with a two-layer MLP mapping hidden states to joint commands, with AdaLN modulators zero-initialized for stability. Action trajectories are generated by iteratively refining Gaussian noise using DDPM-style sampling [31], [32], [33].

V. Tenma for Bi-Manual Tasks

For bi-manual arm control, we use an observation history of $h = 2$ timesteps $(o_{t-h+1:t})$ and predict an action horizon of $n = 16$ steps $(a_{t:t+n-1})$, enabling short-term context and forward planning within a single inference pass. For model training on bi-manual arm tasks, we adopt a two–stage curriculum: (1) large-scale cross-embodiment pretraining, and (2) task-specific fine-tuning on a dual-arm setup for food-preparation. All training was performed on 8 A100 GPUs.

a) Cross-Embodiment Pretraining: From the **X-Embodiment** corpus [9] we select ∼2k demonstrations spanning 20 tabletop-manipulation tasks and 7 distinct robot embodiments. These include both single-arm and dual-arm systems, ensuring coverage across a wide spectrum of control configurations. Clips are set to 10Hz if timestamps exist, and left at native rate otherwise. This diverse slice supplies rich object variation, bi-manual behaviours, and broad embodiment coverage, equipping Tenma with strong low-level priors

for cross-embodiment and bi-manual arm control before fine-tuning.

b) Domain Fine-tuning: We fine-tune on ∼450 human demonstrations collected with this setup, focusing on long-horizon food-prep tasks. Demonstrations deliberately vary objects, layouts, and lighting, and include perturbations and partial failures to encourage robustness. Each trajectory records (1) synchronized 4-view RGB at 10Hz, (2) end-effector state/action vectors, and (3) ten paraphrased language prompts, yielding multimodal data for adaptation.

TABLE II: Training hyperparameters.

Hyperparameter	Value
Dropout	0.0
Weight decay	0.0
Gradient clipping	None
Learning rate	1×10^{-4}
Batch size	32
Global batch size	256
Warmup steps	500
Precision	BF16
Optimizer	AdamW ($\beta_1 = 0.9$, $\beta_2 = 0.999$, $\epsilon = 10^{-8}$)
EMA	Yes ($\mu = 0.9999$)

VI. Experiments

A. Experiment Setup

We evaluate policy performance across a range of generalization and robustness challenges, focusing on adaptation to generalizability of objects, scenes, and prompts. All experiments follow a fixed evaluation protocol with consistent checkpoints. To ensure realism, we focus on a physical kitchen-inspired setup rather than simulation environment. Because food-preparation tasks involve rich object properties, textures, and contact dynamics, keeping the evaluation grounded in the real world is essential for faithfully testing policy robustness.

We designed four tasks, each targeting a distinct aspect of manipulation:

- **Pour**: Requires precise arm rotation and timing, sensitive to container variation.
- **PickCup**: Tests grasp robustness across cups of different shapes and appearances.
- **PlacePan**: Evaluates spatial reasoning through accurate pan placement on a rack.
- **Stirring**: Challenges long-horizon control, from grasping a thin spoon to sustaining circular motions.

Together, these tasks form a coherent and semantically meaningful domain for studying policy generalization and robustness. Each task and evaluation axis is demonstrated in Figure 1.

B. Hardware Setup

Our experiments use a bi-manual robotic platform composed of two FAIRNO FR5 arms, supported by four Hikvision DS-E12A RGB cameras. The cameras provide complementary viewpoints, with two fixed overhead (high, low) and two wrist-mounted (left, right), offering both global workspace coverage and fine-grained object perspectives.

C. Metrics and Evaluation Axes

We report **Success Rate (SR)** as the primary evaluation metric, defined as the proportion of episodes in which the final task objective is achieved. SR provides a clear and interpretable measure of policy reliability, and is consistent with standard practice in prior work.

To assess Tenma's generalization and robustness, we evaluate SR along three axes that reflect the key distribution shifts in our experimental setup (Table III). These axes capture performance in the nominal setting as well as under object and scene variations.

TABLE III: Evaluation axes for assessing generalization and robustness.

Axis	Description
1. In-Distribution	Standard evaluation on tasks drawn directly from the fine-tuning distribution.
2. Object-Shift	Replace familiar objects with novel instances (e.g., different cups, pans, or spoons) to test intra-task generalization.
3. Scene-Shift	Vary background layouts, lighting conditions, and table configurations to measure spatial robustness.

D. Model Variants and Ablation Study

We evaluate Tenma against three representative diffusion–transformer policies of similar capacity, chosen for strong reported performance and architectural proximity so that comparisons emphasize design choices rather than model size. All comparative models were trained with the hyperparameters provided by the authors' open source implementations. We exclude very large foundation models ($>$ 1B parameters) [1], [2], [4], [6], where scale effects dominate architectural contributions.

TABLE IV: Model size and inference control frequency for the policies compared in the ablation. Parameter counts are approximate; frequencies were measured empirically using the authors' open-source implementations under a common evaluation harness. Higher values (Hz) indicate faster inference.

Policy	Parameters	Freq. (Hz) ↑
DiT-Policy [12]	∼90M	31.0
Diffusion Policy [13]	∼50M	13.9
Octo [3]	∼200M	10.6
Tenma	∼110M	20.2

Tables IV and VI summarize parameter counts, runtime frequency, and key design features. Parameter sizes are broadly comparable across methods. Tenma reaches $\sim$ **20 Hz** with 4 cameras on a RTX 3090 GPU, exceeding *Diffusion Policy* and *Octo* but trailing *DiT-Policy* (31 Hz).

As demonstrated in Table VI, this runtime profile is consistent with architectural differences: Tenma is the only model using a ViT-based encoder (DINOv2-S) rather than lightweight ResNet backbones, and Tenma (like Octo) processes n *observation tokens per timestep*, whereas DiT-Policy

TABLE V: Comparison of Success Rate (SR, %) across baseline models, tasks, and evaluation axes.

Task	In-Distribution				Object-Shift				Scene-Shift			
	Tenma	**DiT-Policy** [12]	**Diffusion Policy** [13]	**Octo** [3]	**Tenma**	**DiT-Policy**	**Diffusion Policy**	**Octo**	**Tenma**	**DiT-Policy**	**Diffusion Policy**	**Octo**
Pour	93.75	14.38	12.30	10.27	61.54	5.49	4.40	3.11	88.10	6.47	5.10	5.25
PickCup	100.00	24.25	17.00	13.50	87.50	7.23	8.32	5.52	100.00	5.16	4.60	7.91
PlacePan	78.38	13.79	11.80	12.88	71.20	4.68	4.29	3.94	70.40	4.33	3.90	3.70
Stirring	83.67	20.04	23.90	14.00	70.00	6.98	9.53	4.36	66.00	3.20	2.90	5.48
Average	**88.95**	18.12	16.25	11.91	**72.56**	6.09	6.64	4.23	**81.13**	4.79	4.13	5.59

TABLE VI: Architectural features of compared policies (n = # an arbitrary number of observation tokens). *DiT-like* means very similar to the formal DiT architecture but with some small technical differences. # Cond. Tokens are the number of tokens that the action tokens are conditioned on.

Policy	Vision Encoder	Decoder	# Cond. Tokens
DiT-Policy [12]	ResNet-18 [26]	DiT [40]	1
Diffusion Policy [13]	ResNet-18	*DiT-like*	1/timestep
Octo [3]	ResNet-50	MLP	$\sim n$/timestep
Tenma	DINOv2-S [29]	DiT	n/timestep

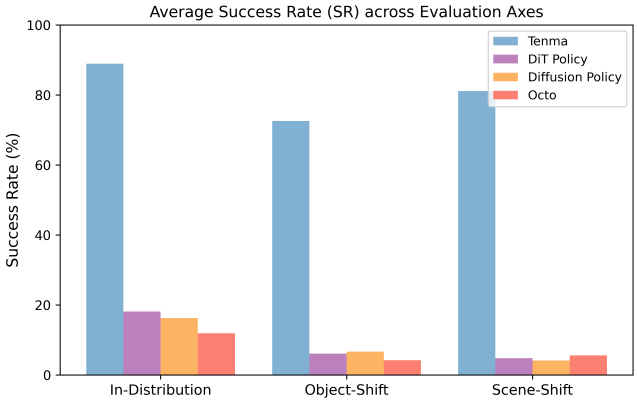

Fig. 4: Visualization of average Success Rate (SR, %) for Tenma and baseline models across three evaluation axes. This figure summarizes the quantitative results reported in Table V, showing that Tenma consistently outperforms all baselines and maintains high performance under distribution shifts.

and Diffusion Policy compress observations to a *single* token, reducing attention cost at potential information loss. Moreover, Octo is not a *DiT-like* policy where it employs a diffusion transformer for denoising, rather it employs a compact ResNet–MLP diffusion head, trading latency for accuracy in our experiments as each model will decode actions an arbitrary number of times. Taken together, these factors indicate that Tenma's $\sim$20 Hz inference frequency reflects a favorable speed–accuracy trade-off given its richer encoder and multi-token representation.

VII. Results

Table V reports Success Rate (SR) across four tasks and three axes (in-distribution, object-shift, scene-shift). **Overall**, Tenma attains an average SR of 88.95% in-distribution and 72.56% / 81.13% under object-/scene-shift, respectively.

Task-specific observations. *Pour* requires a multi-phase sequence (grasp $\rightarrow$ transport $\rightarrow$ tilt/hold $\rightarrow$ pause) with fine control of wrist rotation; object-shift introduces new container geometries (lip/diameter/mass distribution) that alter required tilt profiles, explaining the larger drop (93.75% $\rightarrow$ 61.54%). Under scene-shift, changes in camera pose and target placement are less detrimental (88.10%), suggesting visual grounding is robust once a stable tilt strategy is learned. *PickCup* is a short-horizon grasp-and-lift with moderate pose variation; Tenma maintains near-ceiling SR (ID 100%, object 87.50%, scene 100%), indicating reliable grasp affordances and approach-vector selection even with texture/appearance changes. *PlacePan* involves precise placement onto a target region; errors arise from small pose misalignments and occlusions near the goal. Performance is moderate and relatively uniform across shifts (ID 78.38%, object 71.20%, scene 70.40%), consistent with sensitivity to final alignment rather than object identity. *Stirring* is long-horizon and contact-sensitive (maintaining circular trajectories, bowl depth, and grip on a thin handle); it degrades most under shifts (ID 83.67%, object 70.00%, scene 66.00%), reflecting accumulation of small pose errors and difficulty sustaining stable, periodic motion.

Baselines. DiT-Policy averages 16.87% in-distribution; rollouts frequently reach the object but show hesitation and unstable closures, leading to failures on *PickCup*/*Stirring* and mis-targeting on *Pour*/*PlacePan*. Octo averages 11.91% and often exhibits early task confusion or stalled trajectories, with poor adaptation under both shifts. Diffusion Policy averages 14.25%; executions are steadier than Octo's but commonly end in partial completions (drift, grasp loss), especially on *Pour*/*PlacePan*. These behaviors align with architectural constraints (Table VI): single-token conditioning or shallow decoders limit information flow needed for precise tilt control, final alignment, and sustained periodic motion.

VIII. Discussion

The results indicate that Tenma attains high in-distribution success (avg. SR = 88.95%) and degrades under distribution shifts (object-shift 72.56%, scene-shift 81.13%), consistent with the increased difficulty of novel objects and layouts (Table V). In our evaluation, Tenma outperforms the state-of-the-art baselines (Octo, DiT, Diffusion Policy) across tasks and axes.

Dataset construction likely contributes to these outcomes. For pretraining, we curated a subset of Open X-Embodiment focused on tabletop/food-preparation tasks to ensure diversity of embodiments while maintaining domain coherence. For fine-tuning, we used targeted bi-manual robot demonstrations

with an intentional but imbalanced allocation (e.g., *PlacePan* has 50 episodes versus 100 for other tasks), which plausibly explains its lower in-distribution SR. The overall results are achieved with moderate data scale and a compact policy.

Architectural factors likely account for part of the performance gap. Tenma uses pretrained DINOv2-S (vision), providing stronger perceptual features than the ResNet-based baselines. A cross-embodiment standardizer yields a unified representation that supports stable training across heterogeneous robots, while the Joint State–Time encoder paired with a DiT-based decoder enables fine-grained, temporally coherent action synthesis. By contrast, baselines that employ shallow decoders or compress observations to a single conditioning token (Table VI) introduce information bottlenecks, which is consistent with their observed errors.

Despite using fewer demonstrations than DiT-Policy and Octo and, in Octo's case, a smaller parameter budget, Tenma achieves higher success rates across benchmarks (Tables IV–V). Within our evaluation, this suggests that careful multimodal representation design and targeted data curation can provide greater benefits for scaling of data and model size. Emphasizing learning quality through stronger encoders, cross-embodiment normalization, and multi-token conditioning appears complementary to scale and merits further study.

IX. Conclusion

We presented Tenma, a diffusion-transformer policy that unifies action representation and multimodal conditioning for embodied manipulation. By combining multi-embodiment pretraining, visual–language prompting, and joint state–time attention, Tenma achieves stable and generalizable performance across diverse tabletop tasks. This work demonstrates that robust, generalizable embodied policies can be trained efficiently by filtering pretraining data for domain relevance, leveraging multi-embodiment diversity, and integrating architectural components that jointly capture temporal, spatial, and semantic structure, offering a practical path forward for scalable manipulation learning.

In summary, Tenma achieves this level of performance with modest dataset sizes and model scale, underscoring the efficiency of our approach. Ultimately, Tenma represents a step toward scalable, robust, and adaptable robotic policies, bringing embodied AI closer to deployment in the real world.

References

[1] K. Black et al., π_0*: A vision-language-action flow model for general robot control*, 2024. arXiv: 2410.24164 [cs.LG]. [Online]. Available: https://arxiv.org/abs/2410.24164

[2] S. Liu et al., *Rdt-1b: A diffusion foundation model for bimanual manipulation*, 2025. arXiv: 2410.07864 [cs.RO]. [Online]. Available: https://arxiv.org/abs/2410.07864

[3] O. M. Team et al., *Octo: An open-source generalist robot policy*, 2024. arXiv: 2405.12213 [cs.RO]. [Online]. Available: https://arxiv.org/abs/2405.12213

[4] A. Brohan et al., *Rt-2: Vision-language-action models transfer web knowledge to robotic control*, 2023. arXiv: 2307.15818 [cs.RO]. [Online]. Available: https://arxiv.org/abs/2307.15818

[5] T. L. Team et al., *A careful examination of large behavior models for multitask dexterous manipulation*, 2025. arXiv: 2507.05331 [cs.RO]. [Online]. Available: https://arxiv.org/abs/2507.05331

[6] M. J. Kim et al., *Openvla: An open-source vision-language-action model*, 2024. arXiv: 2406.09246 [cs.RO]. [Online]. Available: https://arxiv.org/abs/2406.09246

[7] H. Touvron et al., *Llama: Open and efficient foundation language models*, 2023. arXiv: 2302.13971 [cs.CL]. [Online]. Available: https://arxiv.org/abs/2302.13971

[8] T. B. Brown et al., *Language models are few-shot learners*, 2020. arXiv: 2005.14165 [cs.CL]. [Online]. Available: https://arxiv.org/abs/2005.14165

[9] E. Collaboration et al., *Open x-embodiment: Robotic learning datasets and rt-x models*, 2025. arXiv: 2310.08864 [cs.RO]. [Online]. Available: https://arxiv.org/abs/2310.08864

[10] AgiBot-World-Contributors et al., *Agibot world colosseo: A large-scale manipulation platform for scalable and intelligent embodied systems*, 2025. arXiv: 2503.06669 [cs.RO]. [Online]. Available: https://arxiv.org/abs/2503.06669

[11] A. Khazatsky et al., *Droid: A large-scale in-the-wild robot manipulation dataset*, 2025. arXiv: 2403.12945 [cs.RO]. [Online]. Available: https://arxiv.org/abs/2403.12945

[12] S. Dasari, O. Mees, S. Zhao, M. K. Srirama, and S. Levine, *The ingredients for robotic diffusion transformers*, 2024. arXiv: 2410.10088 [cs.RO]. [Online]. Available: https://arxiv.org/abs/2410.10088

[13] C. Chi et al., *Diffusion policy: Visuomotor policy learning via action diffusion*, 2024. arXiv: 2303.04137 [cs.RO]. [Online]. Available: https://arxiv.org/abs/2303.04137

[14] R. Yang, G. Chen, C. Wen, and Y. Gao, *Fp3: A 3d foundation policy for robotic manipulation*, 2025. arXiv: 2503.08950 [cs.RO]. [Online]. Available: https://arxiv.org/abs/2503.08950

[15] M. Assran et al., *V-jepa 2: Self-supervised video models enable understanding, prediction and planning*, 2025. arXiv: 2506.09985 [cs.AI]. [Online]. Available: https://arxiv.org/abs/2506.09985

[16] NVIDIA et al., *Gr00t n1: An open foundation model for generalist humanoid robots*, 2025. arXiv: 2503.14734 [cs.RO]. [Online]. Available: https://arxiv.org/abs/2503.14734

[17] C. Chi et al., *Universal manipulation interface: In-the-wild robot teaching without in-the-wild robots*, 2024. arXiv: 2402.10329 [cs.RO]. [Online]. Available: https://arxiv.org/abs/2402.10329

[18] E. Todorov, T. Erez, and Y. Tassa, "Mujoco: A physics engine for model-based control," in *2012 IEEE/RSJ International Conference on Intelligent Robots and Systems*, IEEE, 2012, pp. 5026–5033. DOI: 10.1109/IROS.2012.6386109

[19] V. Makoviychuk et al., *Isaac gym: High performance gpu-based physics simulation for robot learning*, 2021.

[20] NVIDIA, *Nvidia isaac sim*, https://developer.nvidia.com/isaac/sim, Accessed: 2025-07-16.

[21] T. Z. Zhao, V. Kumar, S. Levine, and C. Finn, *Learning fine-grained bimanual manipulation with low-cost hardware*, 2023. arXiv: 2304.13705 [cs.RO]. [Online]. Available: https://arxiv.org/abs/2304.13705

[22] A. Brohan et al., *Rt-1: Robotics transformer for real-world control at scale*, 2023. arXiv: 2212.06817 [cs.RO]. [Online]. Available: https://arxiv.org/abs/2212.06817

[23] T. Davies et al., *Spatially visual perception for end-to-end robotic learning*, 2024. arXiv: 2411.17458 [cs.CV]. [Online]. Available: https://arxiv.org/abs/2411.17458

[24] Y. Huang, T. Davies, J. Yan, X. Chen, Y. Tian, and L. Hu, *Robograsp: A universal grasping policy for robust robotic control*, 2025. arXiv: 2502.03072 [cs.RO]. [Online]. Available: https://arxiv.org/abs/2502.03072

[25] Y. Huang, T. Davies, J. Yan, J. Sun, X. Chen, and L. Hu, *Spatial robograsp: Generalized robotic grasping control policy*, 2025. arXiv: 2505.20814 [cs.RO]. [Online]. Available: https://arxiv.org/abs/2505.20814

[26] K. He, X. Zhang, S. Ren, and J. Sun, *Deep residual learning for image recognition*, 2015. arXiv: 1512.03385 [cs.CV]. [Online]. Available: https://arxiv.org/abs/1512.03385

[27] M. Caron et al., *Emerging properties in self-supervised vision transformers*, 2021. arXiv: 2104.14294 [cs.CV]. [Online]. Available: https://arxiv.org/abs/2104.14294

[28] A. Radford et al., *Learning transferable visual models from natural language supervision*, 2021. arXiv: 2103.00020 [cs.CV]. [Online]. Available: https://arxiv.org/abs/2103.00020

[29] M. Oquab et al., *Dinov2: Learning robust visual features without supervision*, 2024. arXiv: 2304.07193 [cs.CV]. [Online]. Available: https://arxiv.org/abs/2304.07193

[30] C. Raffel et al., *Exploring the limits of transfer learning with a unified text-to-text transformer*, 2023. arXiv: 1910.10683 [cs.LG]. [Online]. Available: https://arxiv.org/abs/1910.10683

[31] J. Ho, A. Jain, and P. Abbeel, *Denoising diffusion probabilistic models*, 2020. arXiv: 2006.11239 [cs.LG]. [Online]. Available: https://arxiv.org/abs/2006.11239

[32] A. Nichol and P. Dhariwal, *Improved denoising diffusion probabilistic models*, 2021. arXiv: 2102.09672 [cs.LG]. [Online]. Available: https://arxiv.org/abs/2102.09672

[33] J. Song, C. Meng, and S. Ermon, *Denoising diffusion implicit models*, 2022. arXiv: 2010.02502 [cs.LG]. [Online]. Available: https://arxiv.org/abs/2010.02502

[34] A. Dosovitskiy et al., *An image is worth 16x16 words: Transformers for image recognition at scale*, 2021. arXiv: 2010.11929 [cs.CV]. [Online]. Available: https://arxiv.org/abs/2010.11929

[35] B. Zhang and R. Sennrich, *Root mean square layer normalization*, 2019. arXiv: 1910.07467 [cs.LG]. [Online]. Available: https://arxiv.org/abs/1910.07467

[36] A. Henry, P. R. Dachapally, S. Pawar, and Y. Chen, *Query-key normalization for transformers*, 2020. arXiv: 2010.04245 [cs.CL]. [Online]. Available: https://arxiv.org/abs/2010.04245

[37] D. Hendrycks and K. Gimpel, *Gaussian error linear units (gelus)*, 2023. arXiv: 1606.08415 [cs.LG]. [Online]. Available: https://arxiv.org/abs/1606.08415

[38] J. Chung, T. Zhu, M. G. Saez-Diez, J. C. Niebles, H. Zhou, and O. Russakovsky, *Unifying specialized visual encoders for video language models*, 2025. arXiv: 2501.01426 [cs.CV]. [Online]. Available: https://arxiv.org/abs/2501.01426

[39] A. Vaswani et al., *Attention is all you need*, 2023. arXiv: 1706.03762 [cs.CL]. [Online]. Available: https://arxiv.org/abs/1706.03762

[40] W. Peebles and S. Xie, *Scalable diffusion models with transformers*, 2023. arXiv: 2212.09748 [cs.CV]. [Online]. Available: https://arxiv.org/abs/2212.09748